Applied Nanoscience (2020) 10:2351–2364
https://doi.org/10.1007/s13204-020-01414-x

ORIGINAL ARTICLE

Green synthesis of magnesium oxide nanoparticles using *Dalbergia sissoo* extract for photocatalytic activity and antibacterial efficacy

Muhammad Isa Khan[1] · Muhammad Naseem Akhtar[1] · Naveed Ashraf[1] · Jawayria Najeeb[2] · Hira Munir[3] · Tahir Iqbal Awan[1] · Muhammad Bilal Tahir[1] · Mohammad Reda Kabli[4]

Received: 23 March 2020 / Accepted: 15 April 2020 / Published online: 25 April 2020

Abstract

Here, the synthesis of magnesium oxide (MgO) nanoparticles (NPs) was carried out by using *Dalbergia sissoo* leaf extract. The synthesis methodology was optimized by studying the effect of reaction parameters on the bandgap (E_g) values of the prepared MgO-NPs. The fabricated NPs were characterized by ultraviolet–visible spectroscopy (UV–Vis), Scanning electron microscopy (SEM), energy-dispersive X-ray spectroscopy (EDX) and X-ray diffraction spectroscopy (XRD). The photocatalytic potential of MgO-NPs was investigated by carrying out the degradation reaction of methylene blue (MB) dye. MgO-NPs with E_g value of 4.1758 eV were found to be most effective in terms of photocatalytic degradation of MB under various conditions. The antibacterial activity of MgO-NPs was also investigated by using the disc diffusion method. MgO-NPs with lower E_g values exhibited better antibacterial results in comparison to the MgO-NPs with higher E_g values. Enhanced antibacterial potential was observed against *Escherichia coli*, while moderate activity was documented against the strain of *Ralstonia solanacearum*. Thus, the engineered MgO-NPs exhibited excellent utility potential for multidimensional applications.

Keywords Magnesium oxide nanoparticles · Photocatalysts · Antibacterial potential · Green chemistry

Abbreviations

MgO	Magnesium oxide
NPs	Nanoparticles
MB	Methylene blue
E_g	Bandgap
UV–Vis	Ultraviolet–visible spectroscopy
SEM	Scanning electron microscopy
EDX	Energy-dispersive X-ray spectroscopy
XRD	X-ray diffraction
D. sissoo	*Dalbergia sissoo*
e^-/h^+	Electron–hole pair
UV	Ultraviolet
%D	Percentage degradation
ZI	Zone of inhibition
R. solanacearum	*Ralstonia solanacearum*
E. coli	*Escherichia coli*

Electronic supplementary material The online version of this article (https://doi.org/10.1007/s13204-020-01414-x) contains supplementary material, which is available to authorized users.

✉ Muhammad Isa Khan
muhammad.isa@uog.edu.pk

✉ Muhammad Bilal Tahir
m.bilaltahir@uog.edu.pk

[1] Department of Physics, University of Gujrat, Gujrat, Pakistan

[2] Department of Chemistry, University of Gujrat, Gujrat, Pakistan

[3] Department of Biochemistry and Biotechnology, University of Gujrat, Gujrat, Pakistan

[4] Department of Industrial Engineering, Faculty of Engineering, King Abdulaziz University, Jeddah, Saudi Arabia

Introduction

Nanotechnology, manipulation of functional materials having at least one of its dimensions in the nanometers at the atomic or molecular scale, has emerged as an promising multidisciplinary research field in recent times owing to its advanced applications in almost every domain of life (Esfe et al. 2015). Numerous methodologies including physical, chemical and electrochemical routes have been reported in the academic literature for the synthesis of nanomaterials (Kamalakkannan et al. 2016). However, most of the physical

methods require experimental setups with high energy consumption values, extreme working conditions, complicated templates, etc. (Alrashed et al. 2018; Sarafraz et al. 2018). Chemical/electrochemical approach suffers from the drawbacks such as the utilization of noxious organic solvents (Hosseini et al. 2017) and hazardous reducing agents (Karimipour et al. 2018), production of harmful by-products and additional electrical setups (Safaei et al. 2016). Owing to these reasons, the focus regarding the synthesis methodologies has now been shifted toward the biochemical synthesis of nanomaterials (Guimarães et al. 2020). This methodology utilizes eco-friendly natural extracts of biomass (such as plants, fungi, bacteria, and algae) as an alternative to harmful chemicals used in the case of chemical/electrochemical methodologies. Advantages (such as the environment-friendly nature of raw materials, low cost/cheap precursors, simple synthetic steps and high efficacy) associated with this green approach has ushered a scientific approach regarding the synthesis methodologies into the new era of safe/non-toxic approach for the production of nanomaterials (Solano et al. 2019; Din et al. 2020).

Metal oxides, particularly magnesium oxide (MgO), based nanoparticles (NPs) have been the center of attention for the past two decades owing to their exclusive and unique properties which make them potentially useful in catalysis, sensing, medical and biomedical applications (Salari et al. 2017; Din et al. 2018; Shahsavar et al. 2019). MgO-NPs are generally utilized in the medical field because of its resistive, biocompatible and highly stable nature. Coelho et al. (2019) synthesized MgO-NPs-based hydroxyapatite granules and utilized it as the point of use technology for studying dental infections. They observed that the addition of the nanomaterials improves the antibacterial potential of the composite and hinders the production of biofilm. Sushma et al. (2016) synthesized MgO-NPs by utilizing *Clitoria ternatea* extract and reported enhanced antioxidant potential for the engineered system. Suresh et al. (2018) documented excellent potential for the antibacterial and anticancer activity of MgO-NPs synthesized using the leaf extract of insulin plant.

Apart from the biomedical applications, this particular metal oxide has also been known to exhibit enhanced photocatalytic applications. Degradation studies of numerous dyes including methylene blue (MB) (Aziz and Karim 2019), congo red (Karthik et al. 2019), methyl orange (Dobrucka 2018), etc. have been effectively carried out using MgO-NPs as a photocatalytic system. Bandgap (E_g) values (i.e., the energy difference between the valence and conduction band) provide essential information regarding photocatalytic potential of the engineered nanosystem (Shtarev et al. 2019). This is attributed to the fact that the photocatalytic activity depends on the available electron–hole pair (e^-/h^+) that interact with the molecules present in the medium to carry out photocatalysis (Tahir et al. 2020) and the e^-/h^+ formation as well as recombination reactions is dependent on the E_g values. The detailed calculations of the E_g values can provide insights into the photocatalytic activity of the nanomaterials. As E_g values are also indicative of the size of the NPs, the biological activities that are influenced by the size of the NPs can also be estimated by using these values (Anbuvannan et al. 2019). Literature survey indicates that most of the case studies reporting E_g values document it as a necessary property for the photocatalytic potential after the engineering of the NPs. The synthesis methodologies are not optimized with respect to this property (Anbuvannan et al. 2019; Ashraf et al. 2019; Shkir et al. 2019). Therefore, detailed studies that explore the synthesis methodologies with the focus on E_g values should be carried out for developing a better understanding of the effect of the synthetic parameters on the applicability potential of the nanomaterials.

Keeping the discussed considerations in mind, this study is designed to engineer MgO-NPs by using the biochemical approach The *Dalbergia sissoo* (*D. sissoo*; common name: Sheesham) is an indigenous plant which is famous in Pakistan owing to its ethnomedicinal values (Ali et al. 2019). This common plant has been known to possess numerous phytochemicals that exhibit analgesic, antipyretic, anticancer, antibacterial and osteogenic potentials (Awais et al. 2018). Our research studies on *D. sissoo* also confirm that the metabolites present in *D. sissoo* possess antifungal and antioxidant properties (Munir et al. 2015). The phytochemical profiling of the ethanolic extract of the *D. sissoo* revealed that the extract possesses several biomolecules including sissooic acid, quercetin-3-*O*-rutinoside, kaempferol-3-*O*-rutinoside, dalsissoside, iochanin A, etc. that can be utilized as a stabilizing and reducing agent for carrying out the production of the nanomaterials. Furthermore, in vitro mutagenic and cytotoxicity profiling also evidenced it to be non-mutagenic and non-toxic, respectively (Majeed et al. 2019), which aligns perfectly with the basic rules of green chemistry. Therefore, *D. sissoo* extract was considered as a reductant and stabilizing medium for the production of MgO-NPs in this study.

This research was designed to address the various drawbacks of the conventional approaches used for the production of nanomaterials. Instead of using harmful supporting mediums and reducing agents, the natural extract of *D. sissoo* leaves was utilized for this purpose. Furthermore, the usage of organic solvents for the metabolite extraction was also avoided and an aqueous extract under appropriate laboratory conditions was prepared for carrying out the synthesis of MgO-NPs. Single-step and one-pot synthesis of the MgO-NPs was effectively carried out using *D. sissoo* extract. The reaction was further optimized by using the E_g values, and the sample of MgO-NPs with the most appropriate E_g value was further characterized

using various analytical techniques. To the best of our knowledge, the reported synthetic methodology (by using *Dalbergia sissoo*) for MgO-NPs has not been documented in the academic literature. Furthermore, optimization of the synthesis process with respect to E_g values is also a novel approach that has not been explored in the case of biogenic synthesis of the nanomaterials. This approach of using the E_g value as the deciding factor for optimizing the synthetic route will help in bridging the gap between conventional and biogenic synthesis. Moreover, essential insights into the potential of the synthesized NPs for various applications can also be estimated beforehand by using this methodology.

Materials and methods

Materials

Chemicals including magnesium nitrate hexahydrate ($Mg(NO_3)_2{\cdot}6H_2O$; 99.9%) and MB ($C_{16}H_{18}ClN_3S{\cdot}xH_2O$; ≥ 82%) were acquired from Sigma-Aldrich. For experimental work, double-distilled de-ionized water was utilized. Fresh leaves of *D. sissoo* were acquired from the local botanical area at the University of Gujrat, Pakistan. The specimen sample was further deposited, recognized and authenticated by the Department of Botany, University of Gujrat, Pakistan, as the plant species of *D. sissoo*. All the reagents utilized during the experimental process were of analytical grade.

Synthesis of *D. sissoo* extract

The green extract was synthesized by using double-distilled de-ionized water as the extracting medium. Collected leaves were washed well with water to remove any dust particles attached to the raw sample. The biomaterial was placed under sunlight in dust-free conditions for 4 days. The dried leaves were ground into fine particles using an electrical grinder (Phillips) and the acquired powder was screened through standard stainless steel 60-mesh strainer for ensuring the homogeneity in size of the ground particles. Airtight plastic bags were utilized for the storage of the sample. 5 g of the prepared sample was weighed and added into the container containing 200 mL of water. The reaction container was placed on an electrical hot plate and was further provided with accessories including a magnetic stirrer and thermometer. The temperature of the system was maintained at 80 °C for 4 h with continuous stirring. The mixture was then filtered to remove the solid residue and the extract was poured into airtight sample bottles. The sample bottles were placed in a freezer for storage purposes.

Synthesis of MgO-NPs

In a typical synthesis, 20 mL of *D. sissoo* extract and 5 mL of water were taken in a titration flask and the solution was heated up to 80 °C for efficient extraction. The reaction mixture was then allowed to cool down to 30 °C and 0.1 M solution of $Mg(NO_3)_2{\cdot}6H_2O$ was dropwise added into the reaction assembly. The reaction was allowed to proceed for 4 h. The acquired white precipitates were filtered, washed and dried in an oven for 2 h to get the MgO-NPs. The prepared NPs were stored in an airtight sample bottle. The synthesis methodology was optimized to get better results. The effect of extract concentration on the formation of MgO-NPs was studied by varying the precursor salt to extract concentration ratio from 30:10 to 30:30, while other reaction parameters such as the precursor salt concentration (0.1 M), temperature (30 ± 2 °C) and the pH (3.2 units) were kept constant at that time. Similarly, the effect of precursor salt concentration (at the varying concentrations of 0.001, 0.01, 0.1, 1, and 2 M), pH (at the varying values of 3.2, 6.2, 7.2, and 9.2 units) and temperature (at the varying values of 30, 40, 50, 60, and 70 °C) on the E_g values of MgO-NPs was also studied for optimizing the synthesis methodology.

Characterization

Double beam LAMBDA-3500 UV–visible spectrophotometer (PerkinElmer) was utilized for the primary characterization of the synthesized MgO-NPs. The X-ray diffraction (XRD) was carried out by utilizing D8-Advance diffractometer (Bruker Corporation, USA) working at the optimized conditions of 30 kV, 20 mA and Cu Kα radiations (wavelength = 1.54A°). Scanning electron microscopy (SEM) coupled with energy-dispersive X-ray spectroscopy (EDX) (LYRA3 TESCAN operating at 15 kV) was used for acquiring the micrographs of the synthesized MgO-NPs.

Photocatalytic potential of MgO-NPs

The photocatalytic potential of the synthesized MgO-NPs was investigated by carrying out the degradation of MB under ultraviolet (UV) lamp (10 W with 30mW/cm^2). Before carrying out any photocatalytic experiment, the solution containing 100 mL of 20 ppm MB solution and 10 mg of MgO-NPs was subjected to constant stirring for 40 min to ensure the development of the absorption/desorption equilibrium. Apart from carrying out the reaction under the influence of the UV radiations, similar reactions were carried out under the dark and in the presence of sunlight for comparative analysis. The temperature of 20 ± 4 °C was maintained throughout the experiment. 5 mL of the suspension was removed from the medium after regular intervals and centrifuged for 5 min at 3000 rpm to remove the NPs

from the solution. The separated solution was used for the ultraviolet–visible (UV–Vis) spectral analysis for estimating the concentration of the dye in the reaction medium. Equation 1 was utilized for studying the percentage degradation (%D) of the MB under the specified conditions.

$$\%D = \frac{C_0 - C_t}{C_0} \times 100, \quad (1)$$

where $C_0 - C_t$ represents the difference between the initial and final concentration of the MB at its maximum wavelength, while C_0 shows the amount of the initial MB dye present before the start of the reaction.

Antibacterial potential of the MgO-NPs

The antibacterial potential of the MgO-NPs was investigated against the strains of *Escherichia coli* (*E. coli*) and *Ralstonia solanacearum* (*R. solanacearum*) by utilizing the disc diffusion methodology. Strains of these plant pathogenic species were cultured on the lysogenic nutrient medium poured into Petri dishes at the temperature of 35 °C. The bacterial strains were allowed to grow until sufficient bacterial growth (1.59376 CFU/mL) was acquired. The poured agar solidifies on cooling and the acquired culture was separately charged with 1, 2 and 3 mg/mL of MgO-NPs for investigating the effect of concentration of MgO-NPs on bacterial growth. The cultures were incubated at the temperature of 37 °C at Medicinal Flora Evaluation Characterization and Metabolomics Lab, Department of Botany, University of Gujrat, Pakistan. Kanamycin was utilized as a positive control drug. After 24 h, zones of inhibition (ZI) were measured. Each experiment was replicated three times.

Results and discussion

Synthesis methodology

The synthesis of MgO-NPs was carried out using *D. sissoo* extract (scheme presented in Fig. 1). Certain metabolites including dalsissoside, quercetin-3-*O*-rutinoside,

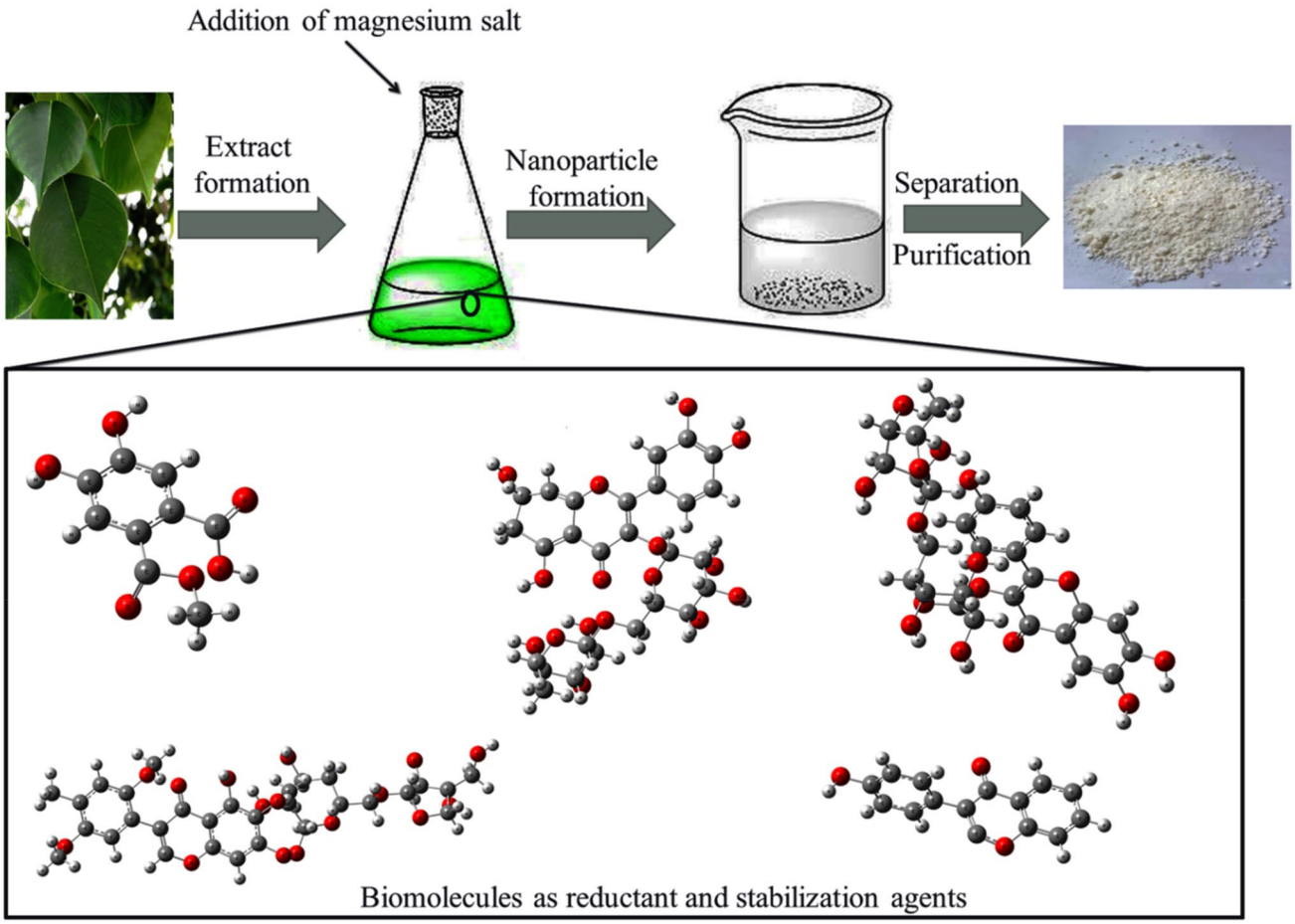

Fig. 1 Schematic representation of synthesis of MgO-NPs sing *D. sissoo* leaf extract

biochanin A, kaempferol-3-*O*-rutinoside, sissooic acid, etc. are reported to be present in the aqueous extract of the *D. sissoo* leaves. Further information regarding the biomolecules present in the extract is provided in the supplementary information. The preliminary confirmation of the formation of the MgO-NPs was acquired by the decrease in the color intensity of the extract. This is ascribed to the fact that the phytochemicals of the plant extract get degraded when carrying out the reduction and stabilization processes for the formation of NPs. Apart from the color transition of the extract (from the dark green to pale white), the appearance of characteristic absorption band affiliated with the MgO-NPs at 268 nm further confirms the formation of the NPs via the utilized green route (as indicated in Fig. 2). Information regarding the shape of the nanostructures is also acquired from the number of peaks present in the UV–Vis spectrum. The appearance of a single peak in the MgO-NPs spectrum suggests that the prepared NPs were iso-morphological (Jeevanandam et al. 2017). The reported spectral range for the characteristic band of MgO-NPs generated owing to the property of surface plasmonic resonance of nanomaterial was documented to be between 258 and 280 nm (Essien et al. 2020). All the synthetic reactions (documented below) that are carried out for the optimization of the synthesis methodology of the MgO-NPs (indicated in Figs. 2, 3, 4, 5) exhibited the characteristic band in the prescribed reported range for MgO-NPs.

Optimization of the methodology

Effect of pH

The reaction methodology was first optimized for estimating the specific pH value required for carrying out the formation of the MgO-NPs. The results acquired from the UV–Vis spectral analysis of the synthesis reaction carried out at different pH values (3.2, 5.2, 7.2, and 9.2) indicated that the pH value of 3.2 is essential for the formation of MgO-NPs. High values of pH inhibit the formation of the small-sized MgO-NPs. This observation is attributed to the fact that the variation in pH values directly affects the nature of charge present at the metabolite species of the extract. This change in the nature of charge affects the binding and reducing capability of the phytochemicals (Ahmed et al. 2016). At low pH values, the active form of the phytochemicals demonstrated the capability to reduce the precursor metal salt, which is in agreement with the nature of the metabolites present in the *D. sissoo* extract. As the metabolites belong to the polyphenolic and flavonoid class, the acidic nature of these compounds was quenched in the basic environment owing to neutralization and hydrolytic reactions. Thus, the greater concentration of the hydroxyl ions in the medium electrostatically favored the aggregation over the reduction processes, leading to the inability of the metabolites to form NPs at higher pH values (Ahmed et al. 2016; Polyakova et al. 2017).

The presence of the characteristics absorption band of MgO-NPs at the wavelength of 268 nm is shown in Fig. 2a. The UV–Vis spectrum of the MgO-NPs was further utilized

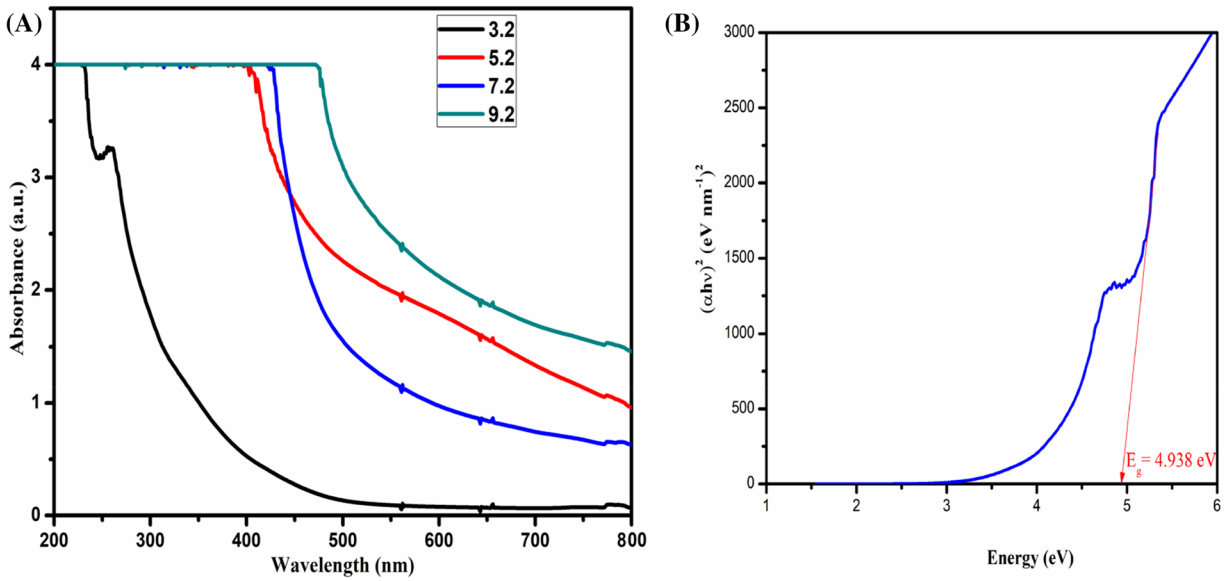

Fig. 2 **a** UV–Vis spectrum for MgO-NPs prepared at different pH values and **b** Tauc plot for MgO-NPs at pH 3.2

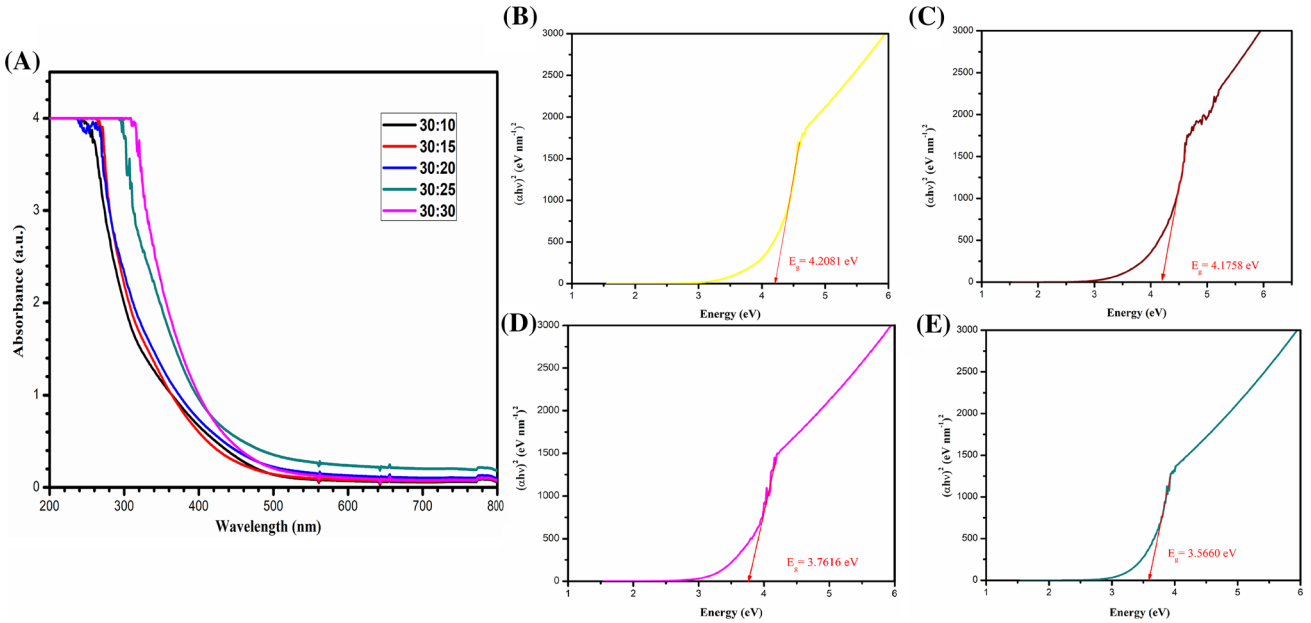

Fig. 3 **a** UV–Vis spectrum for MgO-NPs prepared at different extract concentrations; Tauc plot for MgO-NPs prepared at precursor: extract concentration of **b** 30:15; **c** 30:20; **d** 30:25 and **e** 30:30

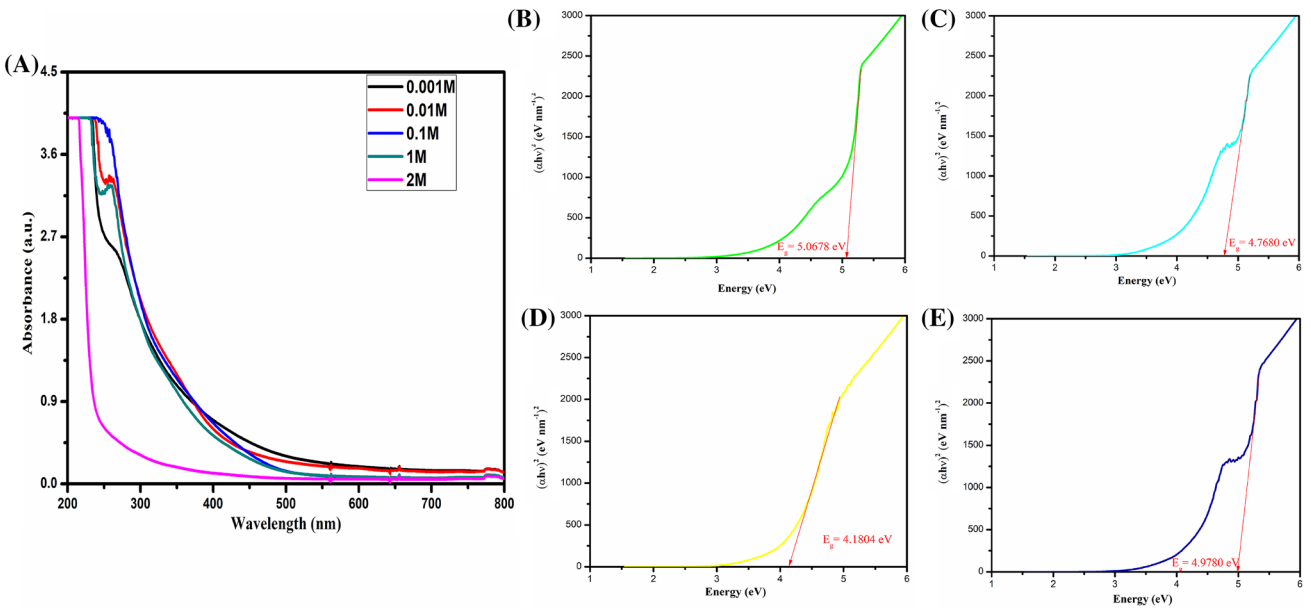

Fig. 4 **a** UV–Vis spectrum for the MgO-NPs prepared at different concentrations of precursor salt; Tauc plot for MgO-NPs prepared at precursor concentration of **b** 0.001 M; **c** 0.01 M; **d** 0.1 M and **e** 1 M

to calculate the E_g values (eV) of the synthesized nanostructures by utilizing the following empirical formula:

$$(\alpha hv)^2 = \left(hv - E_g\right), \tag{2}$$

where hv represents the optical energy, while α represents the absorptivity coefficient of the material (Cheng et al. 2017). The calculated E_g value of 4.938 eV is significant, as this value indicates that MgO-NPs lie within the working range of UV (Kadham et al. 2018). Since the E_g value of the MgO-NPs is greater than 3 eV, these NPs are characterized as wide range NPs. The efficiency of MgO-NPs should be improved by lowering the E_g values. The lowered E_g value will make MgO-NPs more effective in utilizing the broader

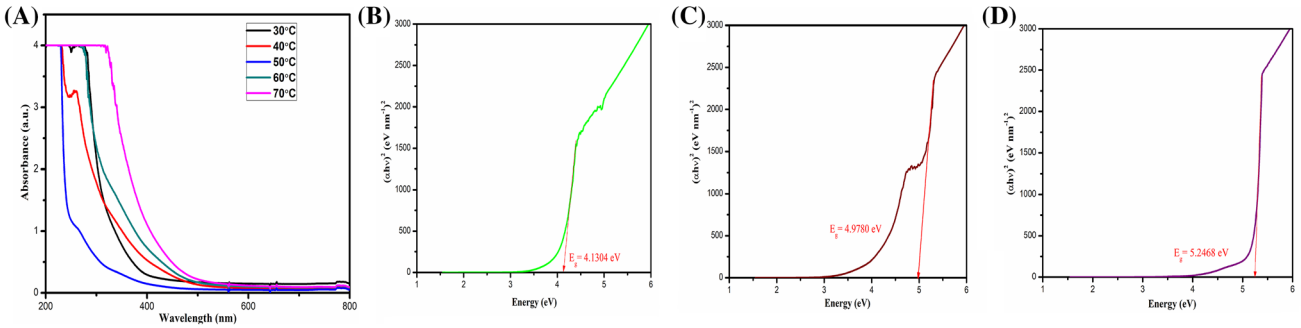

Fig. 5 **a** UV–Vis spectrum for the MgO-NPs prepared at different temperatures; Tauc plot for MgO-NPs prepared at **b** 30 °C; **c** 40 °C and **d** 60 °C

spectrum of electromagnetic radiations in addition to UV radiations for the light-mediated activation of NPs during photocatalysis. Furthermore, the formation of e^-/h^+ will be facilitated by the lowering of the E_g values, which would improve the photocatalytic potential of the synthesized system. However, a very small E_g value will also facilitate the recombination reactions of e^-/h^+ which will lower the concentration of available e^-/h^+ for photocatalytic purposes (Chaudhary et al. 2016). Therefore, the optimized conditions of this synthetic reaction must include those reaction conditions that would facilitate the appropriate lowering of E_g in the case of MgO-NPs. The optimized pH for the synthesis of MgO-NPs by using *D. sissoo* extract was found to be 3.2, as MgO-NPs were not formed at any other pH values.

Effect of extract concentration

The effect of the extract concentration was investigated by varying the ratios of precursor salt to extract volume while keeping all other parameters constant (temperature 30 ± 2 °C, pH 3.2 and precursor salt 0.1 M) as presented in Fig. 3a. Among the prepared samples, samples with the volume ratio of 30:15 and 30:20 exhibited the surface plasmonic resonance peak of the MgO-NPs signifying the effective preparation of MgO-NPs in the medium. The characteristic peak was shifted to higher wavelengths with the increase in the amount of the extract in the reaction medium (i.e., precursor to extract volume ratios of 30:25 and 30:30). At a lower concentration of extract, no peak was observed in the spectrum of MgO-NPs. Results indicated that a moderate amount of the extract was found to be essential for the effective synthesis of MgO-NPs. The small-sized and uniform NPs were formed by utilizing the moderate extract ratios, as a suitable amount of phytochemicals was present in the reaction medium to assist the preparation and stabilization procedure of MgO-NPs. At a lower concentration of extract, few MgO-NPs were formed because the reducing species (phytochemicals from the plant) were not present in an appreciable amount in the reaction medium to carry out synthesis at a suitable rate. However, very small-sized MgO-NPs in large amounts were produced when the amount of extract/phytochemicals in the reaction medium was increased to a considerable level. These small-sized nanostructures owing to their higher instability aggregated to give large-sized MgO-NPs, which are not preferential for the photocatalytic and antimicrobial potentials of the NPs. The presence of the large-sized NPs was further confirmed by the observed color change of the reaction medium. The medium turned from a white solution to a turbid suspension with an increase in the concentration of the extract in the reaction medium (Reda et al. 2019).

The study of the E_g values affiliated with the performed experiments revealed that the increment in extract concentration (from 15 to 30 in the precursor to extract ratios) generated the decrease in the E_g values (from 4.2081 to 3.5600 eV) as indicated in Fig. 3b–e. This observation can be attributed to the following factors associated with the MgO-NPs: the small size of the MgO-NPs was responsible for the presence of numerous oxygen vacancies in the oxide nanostructures; these vacancies provided additional energy levels for the e^-/h^+ transitions and lowered the E_g of the small-sized nanostructures. Similar results were documented by Robles et al. (2019) for zinc oxide NPs. The presence of a large amount of carbon in the reaction medium owing to the phytochemicals also contributed toward decreasing the E_g of the nanostructures (Sadeghi and Dorranian 2016). As the goal of this synthesis is to engineer the nanostructures possessing enhanced photocatalytic potential, the MgO-NPs with 30:20 ratio were considered for further characterization, as the E_g value of these MgO-NPs was found to be 4.1758 eV which was moderate enough for the excitation procedures (e^-/h^+ formation) as well as also suitable for avoiding the e^-/h^+ recombination processes.

Effect of precursor concentration

The effect of precursor concentration was investigated by varying the concentration of $Mg(NO_3)_2{\cdot}6H_2O$ from 0.001 to

2 M while keeping other variables constant. Four out of five samples exhibited the characteristic absorption peak of the MgO-NPs at a wavelength of 268 nm. Figure 4a indicates that the concentration range from 0.001 to 1 M was effective for the synthesis of the MgO-NPs. Utilization of the salt more than this critical concentration (i.e., the concentration at which the reaction rate has become maximum and after this concentration, the reaction rate becomes independent of the understudy concentration factor) is not suggested, as any further increment in the concentration of the salt in the medium inhibits the synthesis of the MgO-NPs. Critical concentration is an industrially useful parameter because it provides an economic workable value of the particular reactant for the synthesis reaction. Furthermore, the reactant with the critical concentration can act as a limiting substance during the chemical synthesis under a particular set of conditions. Application of the critical concentration will not only provide the maximum rate for synthesis, but will also prevent the wastage of the chemical as further addition of salt is not influencing the reaction positively. The critical concentration for the precursor salt for the synthesis of MgO-NPs was found to be 1 M. Besides the acquired information from the UV–Vis spectrum regarding the synthesis of the MgO-NPs (by the appearance of the characteristic band), the absorption value can also be used to carry out the quantitative analysis. The absorbance of the peak is directly proportional to the concentration of the absorbing species in the medium. Since the absorbance at 258 nm acquired by the utilization of the 1 M salt is the maximum, the maximum yield of MgO-NPs was acquired in this reaction in comparison to other concentration values of salt (Chunfa et al. 2018). An exceedingly high concentration of the salt (2 M) was also found undesirable, as the MgO-NPs were not synthesized under this condition. This was attributed to the fact that phytochemicals in the extract were unable to completely reduce the huge number of precursor molecules present in the reaction medium. Furthermore, the reduced nanostructures generated were agglomerated on the unreacted salt molecules present in the reaction medium for achieving surface stability. This led to the formation of very large-sized clusters in the reaction medium, making this reaction condition unsuitable for the synthesis of the MgO-NPs.

Evaluation of the samples revealed that the E_g values calculated by using Tauc plots containing 0.001, 0.01, 0.1 and 1 M salt concentration were found to be 5.0678, 4.7680, 4.1804 and 4.9780 eV, respectively, as presented in Fig. 4b–e. This provided significant insights regarding the state of the MgO-NPs in the reaction medium. At first, the increase in the concentration of the precursor salt (from 0.001 to 0.1 M) resulted in a reduction in the E_g values (from 5.0678 to 4.1804 eV), which is to be expected, as at lower concentrations of the salt, reduction by phytochemicals was quite low because there was a very small amount of salt molecules present in the reaction medium for forming MgO-NPs. This observation was also validated by the low value of absorption intensity observed for the 0.001 M concentration of precursor salt at the characteristic wavelength of the MgO-NPs (consult Fig. 4a). But as the concentration of the salt is increased to the appropriate value, the number of small-sized MgO-NPs present in the reaction medium also increased. This change in the reaction medium was indicated by the reduction in the E_g values of the samples (Robles et al. 2019). As indicated by Fig. 4a, the maximum yield of MgO-NPs was acquired by utilizing the 1 M concentration of the precursor salt (as it possessed the highest absorbance value at 268 nm), but the E_g value of this sample was found to be greater than that of other samples (i.e., 0.01 M and 0.1 M sample). This revealed that the small-sized MgO NPs produced in large amounts got agglomerated to increase the size of the synthesized NPs as indicated by an increase in the E_g value. Thus, the optimized salt concentration for the synthesis of the MgO-NPs was found to be 0.1 M, as an appropriate E_g value of 4.1804 eV was observed for this concentration which is essentially useful for the specified applications of the engineered nanostructures (Reda et al. 2019). The acquired yield of the MgO-NPs will be second highest for 0.1 M concentration, but the prepared MgO-NPs will have appropriate E_g values for carrying out the photocatalytic applications with higher efficacy.

Effect of temperature

The synthesis of the MgO-NPs can further be optimized by varying the reaction temperature of the medium from 30 to 70 °C while keeping all other reaction variables constant. The spectral analysis of the synthesis reaction carried out at numerous temperatures is presented in Fig. 5a. Similar to the factor of pH, the temperature variation directly influenced the reaction constituents of the medium (Giwa et al. 2020). The production of the MgO-NPs by using phytochemicals depended upon the thermal stability of the phytochemicals. If the optimum temperature was not applied during the synthesis, the phytochemicals would break down and would not carry out the process of the reduction and stabilization of the nanostructures (Kumar et al. 2017). Among the performed experiments, only three temperature values including 30, 40 and 50 °C led to the generation of the MgO-NPs as indicated by the appearance of the characteristic absorption peak at 260 nm. Maximum absorbance was observed at the temperature value of 30 °C. Moderate and low absorbance was observed in the case of temperature values of 40 °C and 50 °C respectively.

The E_g values calculated by using Tauc plots for the temperature values including 30, 40 and 50 °C were found to be 4.1304, 4.9780 and 5.2468 eV, respectively, as shown in Fig. 5b–d. The temperature of 30 °C was considered

optimum, as the appropriate E_g value was observed in this case. Furthermore, the yield as indicated by the absorption values was also found to be the maximum for 30 °C. High-temperature conditions not only destabilized the phytochemicals, but also increased the collision frequency of the NPs among themselves, leading to the aggregation of the nanostructures. This was evident from the fact that the MgO-NPs prepared at higher temperature values possessed high values of E_g. At extremely high-temperature values (60 °C and 70 °C), the synthesis of MgO-NPs was completely inhibited by the aggregation phenomenon as revealed by the absence of the characteristic absorption peak of MgO-NPs in the UV–Vis spectrum.

Characterization

XRD analysis carried out for the MgO-NPs is provided in Fig. 6. The MgO-NPs were found to exhibit the solid crystal phase, as evident by the indexing of the diffraction peaks in the XRD data. The acquired diffraction peaks at 2θ values of 36.5°, 42.2°, 62.2°, 75.8° and 78.5° corresponded to the *hkl* values of (111), (200), (220), (311) and (222). which were indicative of the cubic structure of MgO-NPs (JCPDS No. 01-089-7746 and JCPDS No. 01-079-0612). Absence of any additional peak other than the characteristics diffraction peaks of MgO-NPs also affirmed that there was no unreacted reactant present in the sample and the engineered sample also does not contain any other impurity incorporated into its crystal structure. The XRD pattern was further utilized to estimate the crystalline size of the engineered nanoparticles by using the Debye–Scherrer formula (Ghosh et al. 2019) at full width half maximum (FWHM) of the most intense peak at 2θ value of 42.2°. The average size of MgO-NPs prepared under the optimized reaction parameters (i.e., precursor salt to extract ratio of 30:20, pH 3.2, temperature 30 ± 2 °C and 0.1 M precursor salt concentration) was found to be 42 nm.

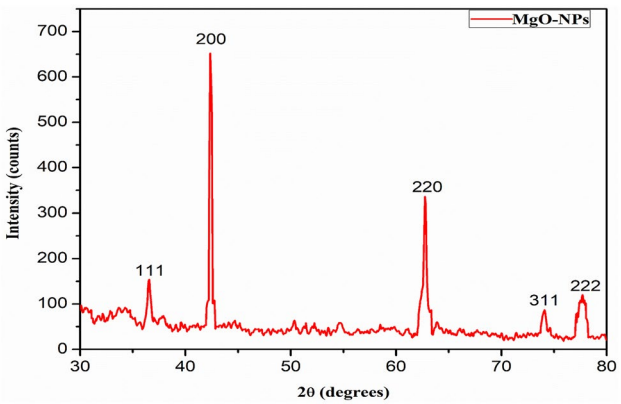

Fig. 6 XRD analysis of MgO-NPs

The SEM micrograph along with EDX analysis of the engineered MgO-NPs prepared under the optimized conditions with the size scale of 0.5 µm (500 nm) is presented in Fig. 7a. The spherical morphology was seen in the topical view of the nanostructures with the average size being below 50 nm. This observation further validated the estimation of the size carried out by the XRD analysis. Agglomeration was also observed at some places as indicated by few large clusters present at the bottom of the SEM micrograph, but it is attributed to the adopted synthetic route and biological incapacitation capabilities of the phytochemicals present in the plant extract. The EDX analysis, presented in Fig. 7b, also confirmed the formation of the MgO-NPs by providing the characteristic peaks for the magnesium and oxygen in the spectrum. The percent weight of the magnesium and oxygen in the MgO-NPs was found to be 37.7% and 62.23%, respectively. The absence of any other peak in the spectrum further suggested that the engineered nanostructures were pure and do not contain any other impurity.

Photocatalytic degradation of MB

The photocatalytic efficacy of engineered MgO-NPs was investigated by carrying out the degradation of MB as shown in Table 1. The information regarding the E_g value provided essential insights into the photocatalytic potential of the MgO-NPs. The maximum degradation efficacy of 81% was

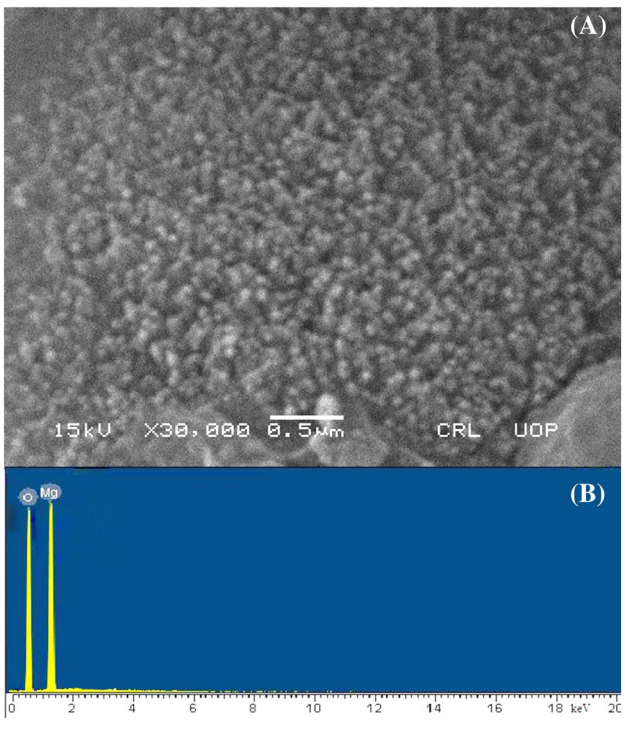

Fig. 7 **a** SEM micrograph of MgO-NPs and **b** EDX analysis of MgO-NPs

Table 1 Degradation reactions carried out for MB using different MgO-NPs samples

Sample number	Reaction conditions	Maximum efficacy under UV-lamp (%)	Calculated bandgap (eV)
S-1	MgO-NPs prepared at temperature 30 ± 2 °C, pH 3.2, precursor salt 0.1 M and salt: extract volume ratio of 30:15	75	4.2081
S-2	MgO-NPs prepared at temperature 30 ± 2 °C, pH 3.2, precursor salt 0.1 M and salt: extract volume ratio of 30:20	81	4.1758
S-3	MgO-NPs prepared at temperature 30 ± 2 °C, pH 3.2, precursor salt 0.1 M and salt: extract volume ratio of 30:25	74	3.7616
S-4	MgO-NPs prepared at temperature 30 ± 2 °C, pH 3.2, precursor salt 0.1 M and salt: extract volume ratio of 30:30	70	3.5660
S-5	MgO-NPs prepared at temperature 30 ± 2 °C, pH 3.2, precursor salt 0.001 M and salt: extract volume ratio of 30:20	65	5.0678
S-6	MgO-NPs prepared at temperature 30 ± 2 °C, pH 3.2, precursor salt 0.01 M and salt: extract volume ratio of 30:20	68	4.7680
S-7	MgO-NPs prepared at temperature 30 ± 2 °C, pH 3.2, precursor salt 1 M and salt: extract volume ratio of 30:20	70	4.9780
S-8	MgO-NPs prepared at temperature 40 ± 2 °C, pH 3.2, precursor salt 0.1 M and salt: extract volume ratio of 30:20	76	4.9780
S-9	MgO-NPs prepared at temperature 50 ± 2 °C, pH 3.2, precursor salt 0.1 M and salt: extract volume ratio of 30:20	70	5.2468

observed for the MgO-NPs having E_g value of 4.1758 eV prepared at the reaction conditions including temperature 30 ± 2 °C, pH 3.2, precursor salt 0.1 M and salt:extract volume ratio of 30:20. However, other MgO-NPs samples also exhibited an appreciable degradation efficacy against MB. An increase in the E_g values as observed in the samples (S-5 to S-9) lowered the degradation efficacy of the MgO-NPs, as more energy was required for the activation of the nanocatalyst via generation of the e^-/h^+ pair (Ansari and Cho 2016). Furthermore, extremely lower E_g values observed in the samples (S-3 and S-4) facilitated the e^-/h^+ pair recombination reactions which decreased the photocatalytic efficacy of the MgO-NPs (Bär et al. 2018). Therefore, the appropriate E_g value as observed in the sample S-2 (where E_g was suitable enough for the activation of the NPs by the electromagnetic radiations and wide enough to avoid the recombination reactions) was required for estimating the photocatalytic efficacy of MgO-NPs. In this study, this appropriate E_g value was found to be 4.1 eV against the dye of MB as indicated in Fig. 8.

Figure 9a provides the UV–Vis spectrum of the MB degradation process carried out using the MgO-NPs prepared at the optimized conditions (S-2). At the start of the experiment, the MB exhibited the characteristic absorption band at 664 nm and less pronounced shoulder band at 615 nm. The absorption values observed for a peak at the 664 nm at any particular time was indicative of the concentration of the MB in the reaction container at that particular time. With the addition of the nanocatalyst, the photocatalysis started and the concentration of MB in the reaction medium started decreasing.

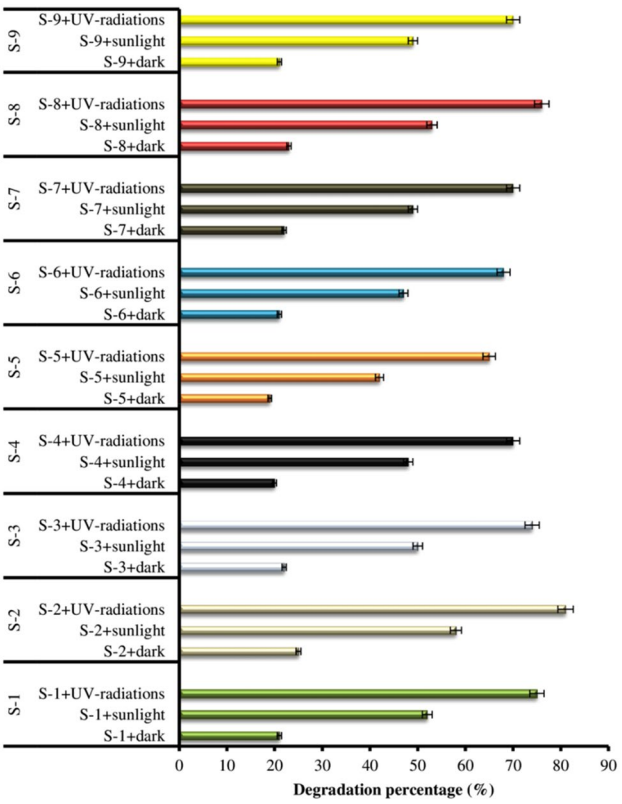

Fig. 8 Photocatalytic degradation of MB using different MgO-NPs samples

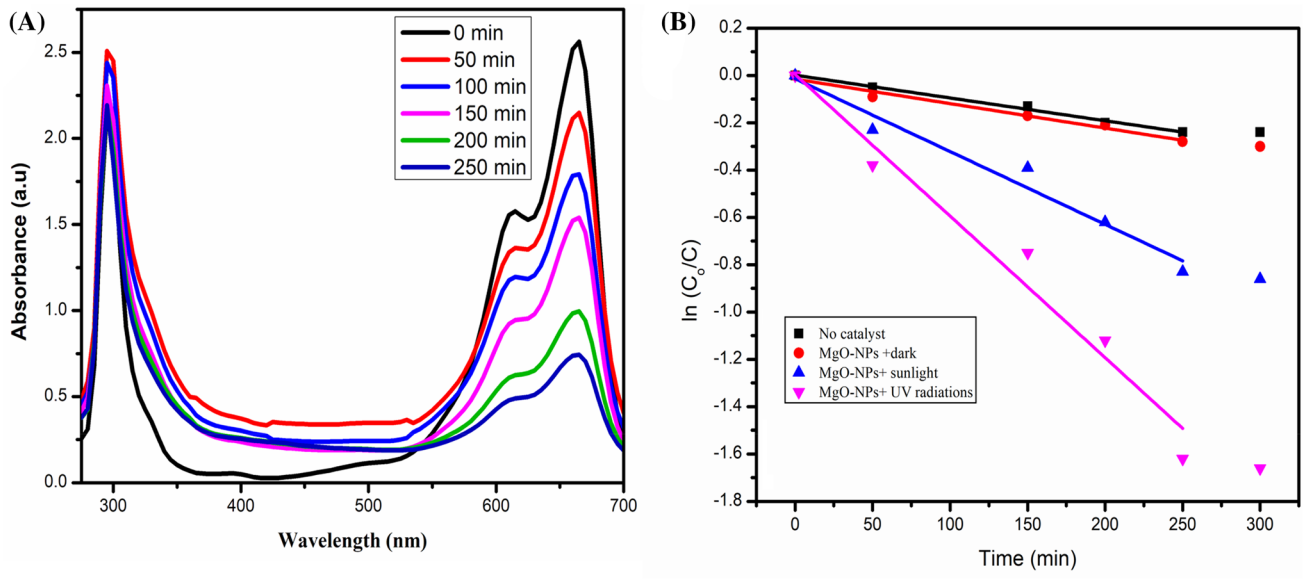

Fig. 9 **a** UV–Vis spectral analysis of the degradation of MB using the MgO-NPs (S-2) and **b** rate constant evaluation by linear regression analysis for the degradation of MB under numerous conditions

Table 2 Inhibition zone values for MgO-NPs against microbes at different concentrations

Microbe	Control	1 mg/mL	2 mg/mL	3 mg/mL
E. coli	15 mm	8 mm	9 mm	11 mm
R. solanacearum	10 mm	5 mm	5 mm	6 mm

Consequently, the absorption values for the characteristic band also decreased with time. After the passage of 250 min, 81% of MB was degraded into its products. The comparative analysis regarding the degradation process under different operating conditions is provided in Fig. 9b. It was observed that in the absence of any catalyst, 16% of the MB was degraded in 250 min. 25%, 58%, and 81% degradation was observed in case of the presence of MgO-NPs in dark, in the presence of sunlight and under UV-lamp (10 W), respectively. The reaction rate constants recorded by using the linear regression analysis were found to be 0.00096 min^{-1}, 0.00103 min^{-1}, 0.00308 min^{-1} and 0.00599 min^{-1} for the reactions performed without any catalyst, MgO-NPs in dark, MgO-NPs in the presence of sunlight and MgO-NPs in the presence of UV-lamp, respectively. The degradation rate constants indicated that the presence of MgO-NPs along with the UV-lamp was essential for achieving the maximum degradation efficacy, but appreciable degradation was achieved by simply carrying out the degradation reaction under sunlight.

Antimicrobial potential of MgO-NPs

The antibacterial potential of MgO-NPs was investigated using the bacterial strains of *E. coli* and *R. solanacearum* as indicated in Table 2. The ZI (the region where the bacterial growth was inhibited owing to the presence of the MgO-NPs) was recorded for numerous samples of MgO-NPs prepared under different conditions. The sample of MgO-NPs produced at the optimized conditions exhibited good results against the strain of *E. coli*. Increment in the concentration of the MgO-NPs positively affected the antimicrobial potential and increased the value of ZI (Ibrahem et al. 2017). However, moderate activity was observed against the strain of *R. solanacearum*. E_g also provided insight regarding the antibacterial potential as the MgO-NPs samples. The MgO-NPs with the lowest E_g values (smallest size) provided the best results against the strain of *E. coli* (consult supplementary information). The processes of lipid peroxidation and generation of reactive oxidative species in the container were responsible for the antibacterial potential of MgO-NPs (Umaralikhan and Jaffar 2018).

Comparison with the academic literature

Comparative analysis of the findings with the recent academic literature further affirms that the biogenic synthetic route used for the MgO-NPs has numerous advantages over the conventional routes. Rukh et al. (2019) carried out the multi-stepped synthesis of the MgO-NPs by using

the hydrothermal methodology. The preparation method required extreme conditions including heating at 220 °C for 48 h and 120 °C for 24 h for effective synthesis of MgO-NPs. Furthermore, hydrogen peroxide which is a noxious reagent was also used as a starting material during the synthesis. Similarly, Fakhri-Mirzanagh et al. (2020) reported a temperature of 550 °C for the synthesis of MgO-NPs by using oleic acid as a capping agent. Our research utilizes the natural extract of *D. sissoo* for carrying out the production of MgO-NPs in almost 8 h with the maximum temperature requirement of 80 °C which indicates the economical and green nature of this synthetic methodology. Furthermore, optimization of the synthetic route with respect to E_g values allowed the synthesis of MgO-NPs with the E_g values ranging from 3.5660 to 5.2468 eV. The E_g values acquired by using this approach was found to be better in comparison to E_g values documented for the microwave (5.93 eV) and hydrothermal (5.85 eV) based synthesis of MgO-NPs (Karthik et al. 2019). The documented rate constant values for the photocatalytic degradation of MB using MgO-NPs were also found to be better than the findings of Aziz and Karim (2019). The antibacterial potential of the MgO-NPs against *E. coli* was also found comparable with the silver/MgO nanocaomposites prepared by using *Musa paradisiaca* extract (Jayapriya et al. 2020).

Conclusion

In this study, MgO-NPs were prepared by using a leaf extract of *D. sissoo* as a reducing and stabilization medium. The synthesis methodology was optimized with respect to E_g values. UV–Vis spectral analysis confirmed the presence of the characteristic absorption band of MgO-NPs within the range of 258-268 nm for the samples prepared under varying conditions. XRD analysis revealed the cubic crystal structure for the MgO-NPs, while SEM analysis revealed the morphology of MgO-NPs to be spherical. EDX analysis indicated that the synthesized samples of MgO-NPs were pure. The MgO-NPs prepared under optimized condition having the E_g value of 4.1 eV exhibited maximum photocatalytic degradation efficiency of 81% against the MB dye. The samples with lower E_g values exhibited improved antibacterial potential against the bacterial strains of *E. coli* and *R. solanacearum*. The MgO-NPs prepared by using *D. sissoo* exhibited enhanced potential for multidimensional applications.

Acknowledgements The authors from University of Gujrat, Gujrat, acknowledge the technical support and facilities provided by the department and university. Dr. Hira Munir acknowledges financial assistance provided by the Higher Education Commission, Pakistan (HEC) under the grant National Research Program for Universities (NRPU) # 6498 for carrying out this research work.

Compliance with ethical standards

Conflict of interest The authors do not have any conflict of interest to declare.

References

Ahmed S, Ahmad M, Swami BL, Ikram S (2016) A review on plants extract mediated synthesis of silver nanoparticles for antimicrobial applications: a green expertise. J Adv Res 7:17–28. https://doi.org/10.1016/j.jare.2015.02.007

Ali I, Rizwani GH, Rasheed M, Ali M, Hassan A, Hassan S, Ishrat G, Zaheer E, Hussain K, Rehman S (2019) Chemical analysis of *Dalbergia sissoo* (Roxb.) pod oil by (GC-MS)/GC-FID and evaluation of antioxidant potential. Pak J Pharm Sci 32:2175–2181

Alrashed AA, Akbari OA, Heydari A, ToghraieD ZM, Shabani GAS, Seifi AR, Goodarzi M (2018) The numerical modeling of water/FMWCNT nanofluid flow and heat transfer in a backward-facing contracting channel. Phys B 537:176–183. https://doi.org/10.1016/j.physb.2018.02.022

Anbuvannan M, Ramesh M, Manikandan E, Srinivasan R (2019) Vitex negundo leaf extract mediated synthesis of ZnO nanoplates and its antibacterial and photocatalytic activities. Asian J Nanosci Mater 2:99–110. https://doi.org/10.26655/AJNANOMAT.2019.1.7

Ansari SA, Cho MH (2016) Highly visible light responsive, narrow band gap TiO_2 nanoparticles modified by elemental red phosphorus for photocatalysis and photoelectrochemical applications. Sci Rep 6:25405. https://doi.org/10.1038/srep25405

Ashraf W, Fatima T, Srivastava K, Khanuja M (2019) Superior photocatalytic activity of tungsten disulfide nanostructures: role of morphology and defects. Appl Nanosci 9:1515–1529. https://doi.org/10.1007/s13204-019-00951-4

Awais M, Gulfraz M, Asad MJ, Kabir F, Khan KS, Naqvi SMZA (2018) Mesophilic anaerobic co-digestion of cattle manure with Malus domestica and *Dalbergia sissoo* during biomethane potential assays. BioResources 13:3144–3156

Aziz BK, Karim MA (2019) Efficient catalytic photodegradation of methylene blue from medical lab wastewater using MgO nanoparticles synthesized by direct precipitation method. React Kinet Mech Catal 128:1127–1139

Bär M, Schnabel T, Alsmeier JH, Krause S, Koch N, Wilks RG, Ahlswede E (2018) CdS/low-band-gap kesterite thin-film solar cell absorber heterojunction: energy level alignment and dominant recombination process. ACS Appl Energy Mater 1:475–482

Chaudhary D, Khare N, Vankar VD (2016) Ag nanoparticles loaded TiO2/MWCNT ternary nanocomposite: a visible-light-driven photocatalyst with enhanced photocatalytic performance and stability. Ceram Int 42:15861–15867

Cheng JL, Mi JY, Miao H, Fatanah BS, Wong SF, Tay BK (2017) Synthesis of ammonium and sulfate ion-functionalized titanium dioxide for photocatalytic applications. Appl Nanosci 7:117–124

Chunfa D, Fei C, Xianglin Z, Xiangjie W, Xiuzhi Y, Bin Y (2018) Rapid and green synthesis of monodisperse silver nanoparticles using mulberry leaf extract. Rare Met Mater Eng 47:1089–1095

Coelho CC, Araújo R, Quadros PA, Sousa SR, Monteiro FJ (2019) Antibacterial bone substitute of hydroxyapatite and magnesium oxide to prevent dental and orthopaedic infections. Mater Sci Eng C 97:529–538

Din MI, Najeeb J, Ahmad G (2018) Recent advancements in the architecting schemes of zinc oxide-based photocatalytic assemblies. Sep Purif Rev 47:267–287

Din MI, Najeeb J, Hussain Z, Khalid R, Ahmad G (2020) Biogenic scale up synthesis of ZnO nano-flowers with superior nano-photocatalytic performance. Inorg Nanomet Chem. https://doi.org/10.1080/24701556.2020.1723026

Dobrucka R (2018) Synthesis of MgO nanoparticles using *Artemisia abrotanum* herba extract and their antioxidant and photocatalytic properties. Iran J Sci Technol A 42:547–555

Esfe MH, Saedodin S, Naderi A, Alirezaie A, Karimipour A, Wongwises S, Goodarzi M, Dahari MB (2015) Modeling of thermal conductivity of ZnO-EG using experimental data and ANN methods. Int Commun Heat Mass 63:35–40

Essien ER, Atasie VN, Okeafor AO, Nwude DO (2020) Biogenic synthesis of magnesium oxide nanoparticles using *Manihot esculenta* (Crantz) leaf extract. Int Nano Lett 10:43–48

Fakhri-Mirzanagh S, Ahadzadeh-Namin K, Givi GP, Farazin J, Azizian-Kalandaragh Y (2020) The effect of capping agent on the structural, optical properties and photocatalytic activity of MgO nanostructures. Phys B 583:412064. https://doi.org/10.1016/j.physb.2020.412064

Ghosh R, Kundu S, Majumder R, Roy S, Das S, Banerjee A, Guria U, Banerjee M, Bera MK, Subhedar KM, Chowdhury MP (2019) One-pot synthesis of multifunctional ZnO nanomaterials: study of superhydrophobicity and UV photosensing property. Appl Nanosci 9:1939–1952

Giwa SO, Sharifpur M, Meyer JP (2020) Effects of uniform magnetic induction on heat transfer performance of aqueous hybrid ferrofluid in a rectangular cavity. Appl Therm Eng 170:115004. https://doi.org/10.1016/j.applthermaleng.2020.115004

Guimarães ML, Silva FAGD, Costa MMD, Oliveira HPD (2020) Green synthesis of silver nanoparticles using *Ziziphus joazeiro* leaf extract for production of antibacterial agents. Appl Nanosci 10:1073–1081

Hosseini SM, Safaei MR, Goodarzi M, Alrashed AA, Nguyen TK (2017) New temperature, interfacial shell dependent dimensionless model for thermal conductivity of nanofluids. Int J Heat Mass 114:207–210

Ibrahem EJ, Thalij KM, Badawy AS (2017) Antibacterial potential of magnesium oxide nanoparticles synthesized by *Aspergillus niger*. Biotechnol J Int 18:1–7. https://doi.org/10.9734/BJI/2017/29534

Jayapriya M, Premkumar K, Arulmozhi M, Karthikeyan K (2020) One-step biological synthesis of cauliflower-like Ag/MgO nanocomposite with antibacterial, anticancer, and catalytic activity towards anthropogenic pollutants. Res Chem Intermed 46:1771–1788. https://doi.org/10.1007/s11164-019-04062-1

Jeevanandam J, Chan YS, Danquah MK (2017) Biosynthesis and characterization of MgO nanoparticles from plant extracts via induced molecular nucleation. New J Chem 41:2800–2814

Kadham AJ, Hassan D, Mohammad N, Ah-yasari AH (2018) Fabrication of (polymer blend-magnesium oxide) nanoparticle and studying their optical properties for optoelectronic applications. Bull Electr Eng Inform 7:28–34. https://doi.org/10.11591/eei.v7i1.839

Kamalakkannan J, Chandraboss V, Loganathan B, Prabha S, Karthikeyan B, Senthilvelan S (2016) $TiInCrO_6$-nanomaterial synthesis, characterization and multi applications. Appl Nanosci 6:691–702

Karimipour A, Bagherzadeh SA, Goodarzi M, Alnaqi AA, Bahiraei M, Safaei MR, Shadloo MS (2018) Synthesized $CuFe_2O_4/SiO_2$ nanocomposites added to water/EG: evaluation of the thermophysical properties beside sensitivity analysis & EANN. Int J Heat Mass 127:1169–1179

Karthik K, Dhanuskodi S, Gobinath C, Prabukumar S, Sivaramakrishnan S (2019) Fabrication of MgO nanostructures and its efficient photocatalytic, antibacterial and anticancer performance. J Photochem Photobiol B 190:8–20

Kumar V, Singh K, Panwar S, Mehta SK (2017) Green synthesis of manganese oxide nanoparticles for the electrochemical sensing of *p*-nitrophenol. Int Nano Lett 7:123–131

Majeed FA, Munir H, Rashid R, Zubair MT (2019) Antimicrobial, cytotoxicity, mutagenicity and anti-epileptic potential of ethanol extracts of a multipurpose medicinal plant *Dalbergia sissoo*. Biocatal Agric Biotechnol 19:101155

Munir H, Shahid M, Subhani Z, Afzal M, Pirzada T (2015) Antimicrobial and antioxidant activities of hydrolysed and modified Gum Acacia modesta and *Dalbergia sissoo*. Oxid Commun 38:1632–1644

Polyakova NY, Polyakov AY, Sukhorukova IV, Shtansky DV, Grigorieva AV (2017) The defining role of pH in the green synthesis of plasmonic gold nanoparticles using Citrus limon extract. Gold Bull 50:131–136

Reda M, Ashames A, Edis Z, Bloukh S, Bhandare R, Sara HA (2019) Green synthesis of potent antimicrobial silver nanoparticles using different plant extracts and their mixtures. Processes 7:510. https://doi.org/10.3390/pr7080510

Robles CAS, Luque PA, Gutiérrez CMG, Nava O, Nestor ARV, Medina EL, Ranjithukmar R, Beltrán AC (2019) Study on the effect of the concentration of *Hibiscus sabdariffa* extract on the green synthesis of ZnO nanoparticles. Results Phys 15:102807. https://doi.org/10.1016/j.rinp.2019.102807

Rukh S, Sofi AH, Shah MA, Yousuf S (2019) Antibacterial activity of magnesium oxide nanostructures prepared by hydrothermal method. Asian J Nanosci Mater 2:425–430

Sadeghi H, Dorranian D (2016) Influence of size and morphology on the optical properties of carbon nanostructures. J Theor Appl Phys 10:7–13

Safaei MR, Ahmadi G, Goodarzi MS, Shadloo MS, Goshayeshi HR, Dahari M (2016) Heat transfer and pressure drop in fully developed turbulent flows of graphene nanoplatelets–silver/water nanofluids. Fluids 1:20. https://doi.org/10.3390/fluids1030020

Salari E, Peyghambarzadeh S, Sarafraz M, Hormozi F, Nikkhah V (2017) Thermal behavior of aqueous iron oxide nano-fluid as a coolant on a flat disc heater under the pool boiling condition. Heat Mass Transf 53:265–275

Sarafraz M, Nikkhah V, Nakhjavani M, Arya A (2018) Thermal performance of a heat sink microchannel working with biologically produced silver-water nanofluid: experimental assessment. Exp Therm Fluid Sci 91:509–519

Shahsavar A, Khanmohammadi S, Karimipour A, Goodarzi M (2019) A novel comprehensive experimental study concerned synthesizes and prepare liquid paraffin-Fe_3O_4 mixture to develop models for both thermal conductivity & viscosity: a new approach of GMDH type of neural network. Int J Heat Mass 131:432–441

Shkir M, Chandekar KV, Alshehri BM, Khan A, AlFaify S, Hamdy MS (2019) A remarkable enhancement in photocatalytic activity of facilely synthesized Terbium@ Zinc oxide nanoparticles by flash combustion route for optoelectronic applications. Appl Nanosci. https://doi.org/10.1007/s13204-019-01236-6

Shtarev DS, Shtareva AV, Ryabchuk VK, Rudakova AV, Serpone N (2019) Considerations of trends in heterogeneous photocatalysis. Correlations between conduction and valence band energies with bandgap energies of various photocatalysts. ChemCatChem 11:3534–3541

Solano RA, Herrera AP, Maestre D, Cremades A (2019) Fe-TiO2 nanoparticles synthesized by green chemistry for potential application in waste water photocatalytic treatment. J Nanotechnol. https://doi.org/10.1155/2019/4571848

Suresh J, Pradheesh G, Alexramani V, Sundrarajan M, Hong SI (2018) Green synthesis and characterization of hexagonal shaped MgO

nanoparticles using insulin plant (*Costus pictus* D. Don) leave extract and its antimicrobial as well as anticancer activity. Adv Powder Technol 29:1685–1694

Sushma NJ, Prathyusha D, Swathi G, Madhavi T, Raju BDP, Mallikarjuna K, Kim HS (2016) Facile approach to synthesize magnesium oxide nanoparticles by using *Clitoria ternatea*—characterization and in vitro antioxidant studies. Appl Nanosci 6:437–444

Tahir MB, Ashraf M, Rafique M, Ijaz M, Firman S, Mubeen I (2020) Activated carbon doped WO_3 for photocatalytic degradation of rhodamine-B. Appl Nanosci 10:869–877

Umaralikhan L, Jaffar MJ (2018) Green synthesis of MgO nanoparticles and it antibacterial activity. Iran J Sci Technol A 42:477–485